ACC 2024

Aircraft Design Report

of Tsinghua University Team

Team Name: **THU AIR**

Team Number: **No.24**

Team University: **Tsinghua University**

Finish Date: 2024-4-30

Content

1 Introduction

1.1 Tsinghua University and the Organization "AIR"

Established in 1911, Tsinghua University is China's preeminent institution, leading scientific and engineering research advancements.

The Center of Aero Innovation & Realization for Students (AIR) is a distinguished student association within the School of Aerospace Engineering at Tsinghua University. It is dedicated to creating a supportive environment for undergraduate and graduate students with state-of-the-art facilities and tools essential for developing and realizing aeronautic projects. Additionally, AIR advantages from the expertise of professionals from the School of Aerospace Engineering, who serve as consultants, further enriching the students' academic and practical learning experience.

Figure 1.1 ACC2011, ACC2013, ACC2015 and ACC2017

1.2 The Team

Dongyun Ge: Associate professor of aircraft structure design. Team leader. Adviser of THU-AIR.

Shiyu Qian: Senior, majoring in Aircraft Engineering. Finance and Sponsorship. Participant in ACC2022.

Liuyi Wang: Junior, majoring in Mechanical Engineering. Team management, structural design, preliminary design, aerodynamic design, and CNC manufacturing.

Bohong Su: Sophomore, majoring in Mathematics. Aerodynamic design and pilot.

Zhijiang Chu: Junior, majoring in Theoretical and Applied Mechanics. Structural design.

Mingcheng Lei: Sophomore, majoring in Mechanical Engineering. CFD calculation.

Hongchen Li: Junior, majoring in Theoretical and Applied Mechanics. Landing gear and composite material processing.

Haochen Fu: Sophomore, majoring in Aircraft Engineering. Propulsion system.

2 Project Management

2.1 Financial Budget

Financial budge	Items	Expenses
Preparation	Materials	€2000
	Manufacture	€600
	Molds	€800
	Test flight	€500
	Others	€200
Competition		
	Registration fee	€700
	Airplane tickets	€8000
	Accommodation	€1000
	Others	€200
Total		€14000

2.2 Time Schedule

The time schedule is presented as following:

Task list	Nov	Dec	Jan	Feb	Mar	Apr	May	Jun	Jul
Team formation	■	■							
Exploring craftsmanship	■	■	■	■	■	■	■		
Testing propulsion system		■	■						
CFD and airfoil design			■	■	■				
Test model				■	■	■	■	■	

Preliminary report									
Test flight									
Design adjustment									
Report									
Model building									
Soliciting sponsorships.									
Packing up									
Competition									

2.3 Sponsors and Supporters

Support from sponsors is vital for sustaining this project. During the preparation of this competition, School of Aerospace Engineering and Tsinghua University offered sufficient funding. Besides, the following sponsors and unit also provided reliable components and raw materials.

We would also like to extend our gratitude to our material suppliers, whose contributions of essential components have greatly facilitated our manufacturing processes.

KST Digital Technology limited
Provide high quality small servos

HyboFOAM
Provide PMI foam and other materials.

3 Preliminary Design

3.1 Interpretation of the Rules

Based on the constraints outlined in the ACC 2024 document, we have the following requirements for the aircraft:

- The aircraft needs to fit into a box with a maximum sum of length, width, and height not exceeding 1400mm.
- The aircraft needs to take off within 40m or 60m.
- The aircraft needs to accommodate a data recording box with dimensions of 90x90x30mm, which should have unobstructed view of the sky.
- The payload of the aircraft is a standard billiard ball with dimensions of 57 (+/-1) mm and a mass of 170 (+/-5) g.
- The operating current of the aircraft should not exceed 30A.

- Except during takeoff and landing, the flight altitude should not be lower than 10m or higher than 100m.

Additionally, in terms of scoring, the performance requirements for the aircraft are divided into efficiency, payload, and speed. Therefore, we need a design with smaller wingspan, higher wing loading, and a streamlined fuselage.

3.2 Thrust System

Under the current conditions, we first used the thrust testing rig (as shown in the figure) to conduct the following tests on various propellers:

1.Push the thrust control lever to 1/2, 3/4, and full positions respectively to measure the thrust.

2.Test the current and thrust of the propeller of this model under four different conditions.
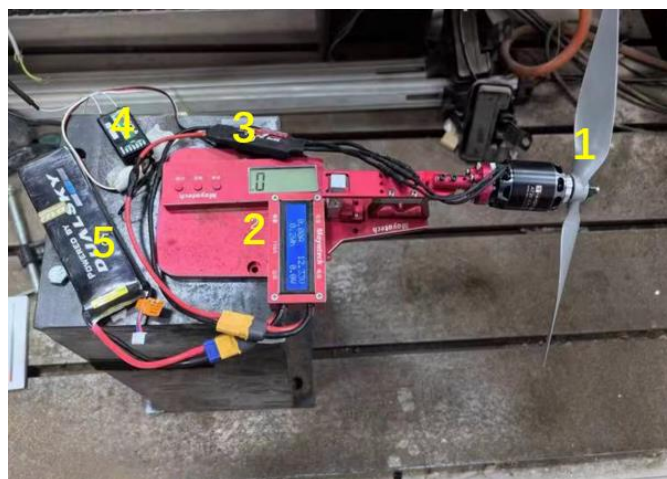
1.   Fixed motor and propeller 2. Ammeter 3.ESC 4. Battery 5. Base
Figure3.2 Thrust test bench

prop	half power	3/4 power	full power
JFX12×6	10A,733g	21A,1309g	33A,1784g
JXF11×5	6.7A,403g	17A,1050g	26A,1422g
APC 12×5	11A,702g	23A,1131g	38A,1601g
APC 10×10	9.1A,415g	24A,930g	32A,1110g
APC 10×8	5.2A,333g	17A,830g	26A,1228g
APC 11×8	6.2A,404g	19A,1092g	31A,1533g
APC 12×8	6.6A,510g	21A,1266g	38A,1826g
APC 11×10	11A,619g	21A,1171g	29A,1393g

Table 3.2 Actual measurement of power system operating current and thrust

It can be seen from Table 3.2 that although the static thrust of propellers above 12 inches is considerable, it exceeds the current limit of 30A on the ground. Therefore, 11 inches is selected. When the propeller diameter is the same, the static thrust changes with the propeller pitch. The improvement first increases and then decreases, among which

APC11x8 delivers the best static thrust. Within the acceptable range of penalty for exceeding the current limit, we will choose a propeller that can work at higher speeds. Additionally, during the test flight, we choose the 11x8 propeller which seems to have substantial static trust and still had some margin during takeoff. Hence, our team decided to use the 11x10 plastic propeller.

This time the competition mandates the use of T-motor AT2826, with a current limit of 30A. With a fully charged 12.3V battery, our maximum output power should be controlled within 369W. Considering the typical efficiency of an ESC-motor system is 80-90%, the input power to the propeller should be around 300-320W. Taking into account that the propeller power increases and then decreases with speed when the speed is the same, if we can tolerate the penalty for a few seconds of overcurrent during acceleration, we can use a propeller that can work at higher speeds. Based on this principle, we selected the APC11×10E propeller as the power source during the selection phase and obtained its fitted thrust curve as follows.

Using the performance data provided by the manufacturer (apc.com), we developed a model
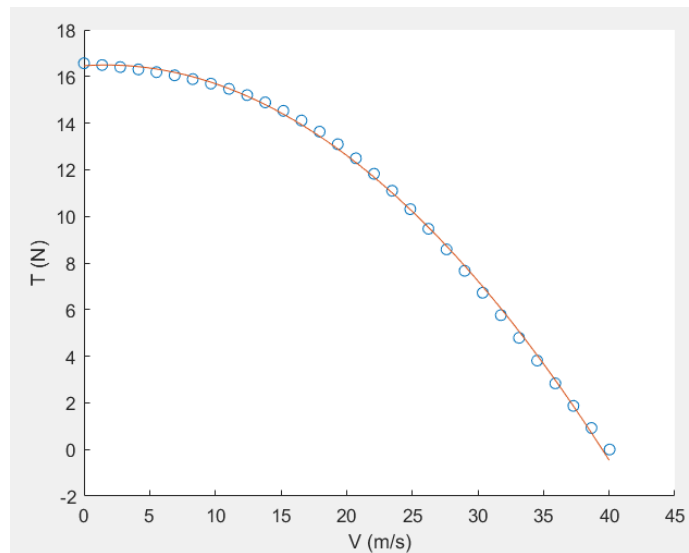
$$T = 16.46 + 0.03856V - 0.01154V^2$$

Figure3.2 APC11*10 Thrust Data

The propeller fixed on the fuselage was measured on the ground, and it was found that the thrust was still 16.5N when at stationary, with almost no thrust loss. This confirms that he results based on our estimation method is consistent with the performance data from the official website.

3.3 Size Estimate

Considering the packing dimensions and the diameter of the payload ball (57mm), the thickness of the fuselage (above 60mm), and the width (above 120mm), along with the estimated static thrust of around 16N from section 3.2, we estimate the total weight to be around 4-5kg, based on a thrust-to-weight ratio of approximately 0.3. Therefore, the

payload capacity should not be less than 12 balls. Additionally, we are pursuing a high aspect ratio and a relatively longer tail moment arm, requiring sufficient space for the payload balls. The wingspan should be controlled to be above 2000mm, and the fuselage length should not be less than 1000mm. Considering the typical design wing loading for low-speed model aircraft (around 80-90g/dm²), the wing area would be approximately 0.5-0.6m², with a chord length of 250-300mm.

3.4 Motor-Fuselage Configuration

In order to reduce drag and improve flight efficiency, maintaining a clean propeller slipstream is often necessary. One method used is to employ a pusher configuration.

Figure3.4 a conceptual aircraft with pusher configuration

Due to the high density of the payload ball and the small space in the fuselage, it can be completely placed behind one-third of the area of the propeller disk center, almost without obstructing the high-speed wake. The propeller area is $A_{pro} = 61314mm^2$, and the maximum fuselage area, taken as the area of a rounded rectangle that can accommodate two balls side by side, is approximately $A_{fus} = 10000mm^2$. The blockage ratio is calculated as $B = \frac{A_{fus}}{A_{pro}} = 16.31\%$.

The estimated value of the critical blockage ratio is typically between 0.33 and 0.42. If the blockage ratio is above the critical value, the efficiency will decrease by 1% for every 10% increase in blockage, with a typical reduction rate of about 5%. This is due to the slipstream effect in tractor-configured light general aviation aircraft. This aircraft can be designed without considering the slipstream effect.

It was also found through testing that placing the engine at the front of the fuselage does not result in thrust loss. However, a rearward position with twin tail booms makes it difficult to maintain the center of gravity, increases structural complexity, and the need for a higher landing gear limits our ability to adopt a shorter takeoff distance using a tailwheel configuration. Therefore, the front-pull power layout remains the chosen configuration.

The estimation of the fuselage drag is crucial when the entire fuselage is subjected to severe turbulence due to the front-pull configuration. The volume Reynolds number of the fuselage is taken as

$$Re_v = \frac{10^5}{1.5} \cdot V^{\frac{1}{3}}(m) \cdot v(m/s)$$

The fuselage drag is estimated using the formula for fully turbulent flow:

$$Cd_{V-turb} \approx \frac{0.435}{(Re_V)^{1/5}}$$

$$D = \frac{1}{2}\rho v^2 Cd_v V^{2/3}$$

The slipstream velocity v_S of the propeller can be estimated based on the principle of momentum conservation, where v_0 is the inflow velocity:

$$T = \rho v_S(v_0 + v_S/2)A_{pro}$$

Based on this, the fuselage drag can be estimated during takeoff (12m/s), climb (20m/s), and cruise (30m/s) as follows:

Airspeed	12 m/s	20 m/s	30 m/s
Slip flow velocity	23.64 m/s	27.25 m/s	33.11 m/s
Fuselage Re_V (e5)	1.3324	2.2207	3.3310
Cd_V−turb	0.0491	0.0443	0.0409
Drag (N)	0.1177	0.2951	0.6123

Table3.4 Fuselage drag estimation at different speeds

Based on experience, the total lift-to-drag ratio of the wing in cruise conditions is approximately 25. Subsequent calculations have also confirmed this. According to the method described above, the estimated fuselage drags accounts for about one-quarter of the wing drag, which is not a negligible amount. Therefore, it is essential to streamline the fuselage. The next section's global parameter search utilizes the estimated fuselage drag coefficient.

3.5 Global Search

3.5.1 Principles of Estimation

Because the competition has many requirements and limitations, we need to establish a global search framework for calculating scores based on design parameters. First, we need a simple algebraic model for estimating aerodynamic performance. Since the competition is divided into several categories, we will model each process separately. Given that our current discussion does not specify any particular airfoil, we need to provide estimates for a wide range of wing designs. Below are some typical low-speed airfoil polar curves.
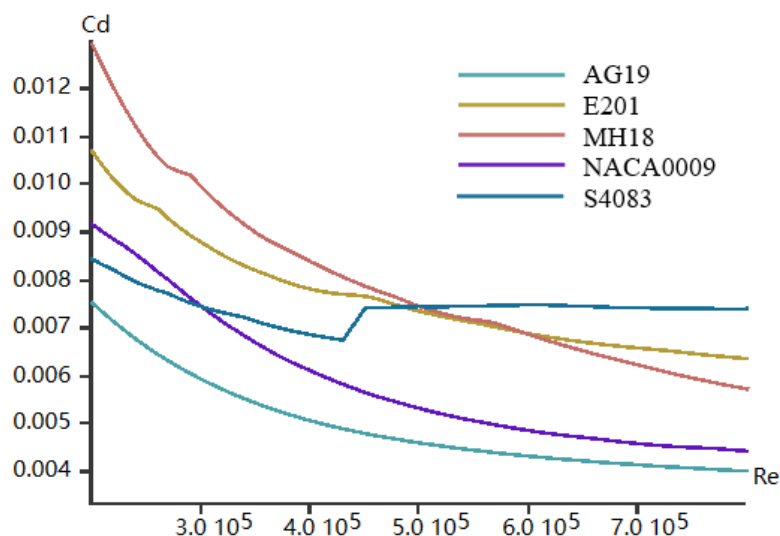
Figure3.5.1-1 Different airfoils exhibit varying drag coefficients at zero angle of attack with changes in Reynolds number.

Due to the existence of induced drag, at a given Reynolds number, the drag of an airfoil that produces lift must be greater than the drag of an airfoil that does not produce lift. According to experience, the drag coefficient of a fully optimized airfoil with appropriate camber and angle of attack can be compared to 1.2-1.5 times the drag coefficient of a simple thin airfoil (such as naca0009) with zero angle of attack at the same Reynolds number. The drag coefficient curve at different Reynolds numbers can be quickly calculated through x5, and the viscous drag change curve can be fitted by intercepting the zero-degree angle of attack data.
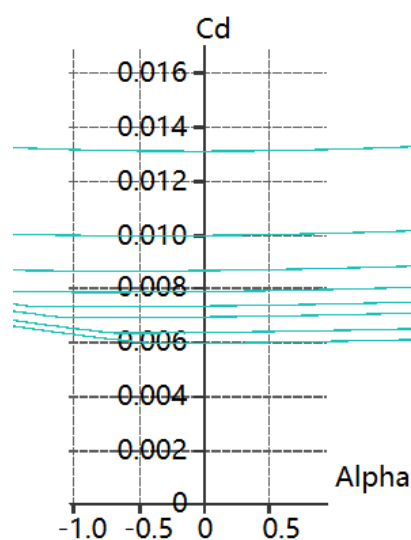

Figure 3.5.1-2 Changes in drag coefficient of NACA0009 at different Reynolds numbers

3.5.2 Takeoff and Climbing

The takeoff and climb phase require meeting the minimum TWR (thrust-to-weight ratio) and climb rate requirements to avoid potential crashes. This phase significantly impacts the aircraft's payload capacity. Additionally, by conducting such calculations, we can estimate the increase in payload capacity with a 60m runway compared to a 40m runway. Our conclusion is that the 5% bonus score is still very important, so we should try to use the 40m runway for takeoff if possible.

During the takeoff and climb phase, based on the experience from previous competitions, we have developed a simple program to estimate that, for the same aerodynamic parameters (assuming the same aircraft), the total score in the competition is not significantly correlated with the payload. However, increasing the payload will significantly increase the takeoff distance, leading to difficulties in takeoff. This also imposes high structural requirements. Additionally, due to the requirement for flight speed, we cannot use wing profiles with excessive curvature.

For the takeoff phase, we can establish the following dynamic model:

$$m\frac{dv}{dt} = T(v) - D(v)$$

In the previous section, we obtained the thrust. Here, we analyze the components of drag during takeoff:

$$D = D_{friction} + D_{ind} + D_{vics} + D_{fus}$$

Ground friction

$$D_{friction} = mg\mu\left(1 - \left(\frac{v}{v_{takeoff}}\right)^2\right)$$

Induced drag is proportional to lift squared

$$D_{ind} = \frac{L^2}{\frac{1}{2}\pi e\rho v^2 Span^2}$$

Viscous drag is estimated using $CL_{takeoff}$.

Shape drag relative to other components of the fuselage is estimated using the following empirical formula

$$D_{fus} = \gamma V^2$$

At the same time, considering the takeoff lift coefficient $CL_{takeoff} = 1.2$ of the aircraft under 15° flaps, the taxiing distance can be obtained

$$s = \int vdt = \int_0^{v_{takeoff}} v\frac{mdv}{T - D}$$

It is necessary to limit $s \leq 40m$ in optimization

Takeoff speed is determined by lift equal to gravity when lifting off the ground.

$$L_{takeoff} = \frac{1}{2}\rho v_{takeoff}^2 CL_{takeoff} = mg$$

In the same way, the climb angle and climb rate can be obtained

11

$$mg \sin \theta = T(v_{climb}) - D(v_{climb})$$
$$r = v_{climb} \sin \theta$$

Since the first stage of the competition is the 90-second efficiency flight phase, which requires flying with the lowest possible energy consumption during this period, it is necessary to climb to a sufficient altitude within the 30-second interval from successful takeoff to the start of high-speed flight in order to fully utilize gravitational potential energy for gliding. The height that can be climbed during this period can be calculated as follows:

$$H_{climb} = r(30 - t_{accelerate})$$

The calculated climb height within 30 seconds is shown in Figure 3.6.1, with values exceeding 100m recorded as 100m.
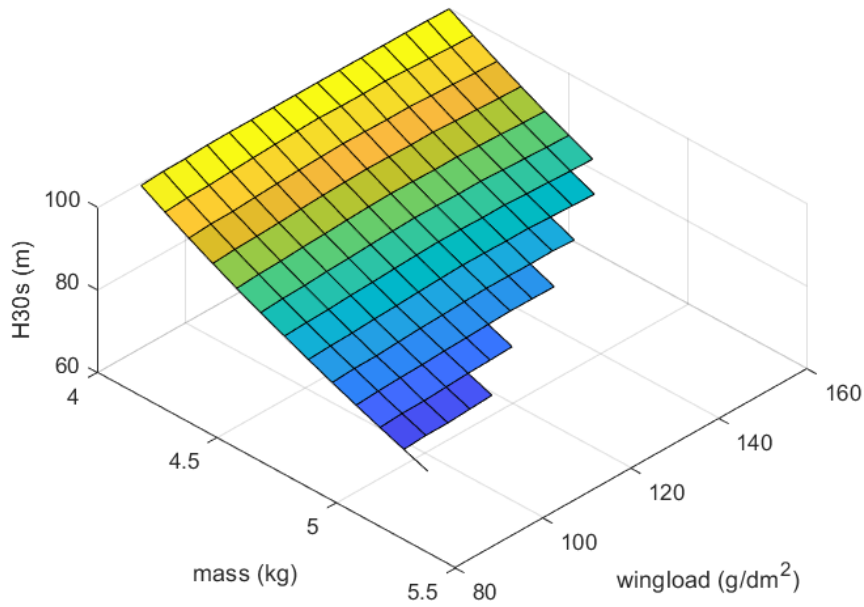
Figure3.5.2 Climb Height within 30 Seconds

3.5.3 Efficient Flight

The efficiency flight phase begins immediately after the climb phase.

The score formula of the efficiency stage generally reflects the power consumption per unit distance, and at the same time avoids the infinite score caused by the use of unpowered gliding mode. According to experience, the thrust of the propeller will be sharply lost at high speed, and the efficiency will also drop significantly. However, for the increase in speed is weak, so it is unwise to try to push up the throttle to increase the flight distance, so the problem is to find the most efficient cruising speed.

Using energy algorithm, the total energy consumed to maintain the balance of thrust and drag during flight

$$E_{out} = DV_{eff} * 90 - mg(H_{climb} - H_{min})$$

The minimum flight altitude H_{min} is limited by competition, safety and pilot experience, and is taken as 25m here.

Flight resistance is still estimated by the following formula

$$D = D_{ind} + D_{vics} + D_{fus}$$

Where $D_{fus} = \left(1 + 0.5\frac{m-3.1}{3}\right) * 0.0035 V_{eff}^2$

And CD_{visc} is obtained by interpolating the Xflr5 data.

The output efficiency of the system consists of three parts

$$\eta = \eta_{prop}\eta_{ESC}\eta_{motor}$$

System consumption is the power input from the battery

$$E_{consumed} = \frac{E_{out}}{\eta}$$

Based on this calculation, the team scores for individual projects are shown in the figure below. It can be seen that a high wing loading and a relatively low takeoff weight can achieve the highest individual scores.
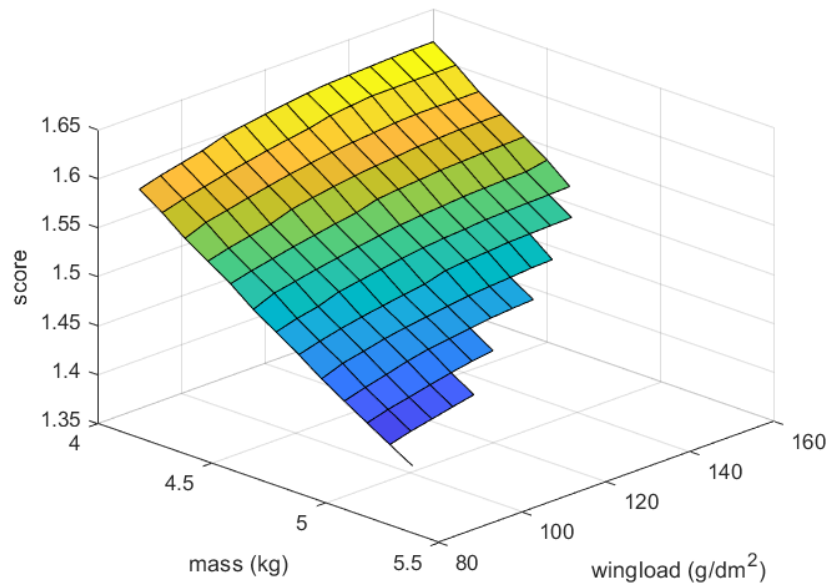
Figure3.5.3 the score of Efficient flight

3.5.4 Distance Flight

At the end of the efficiency flight phase, the 90-second distance flight phase begins. Since the time is fixed, this period of time is the average ground speed of competing aircraft. When the battery power is sufficient, the maximum flight speed can be found and maintained.
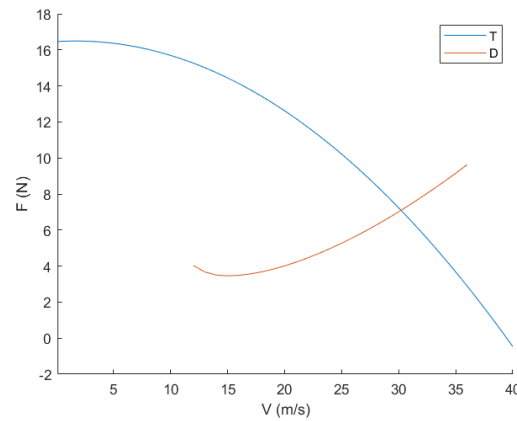
Figure 3.5.4 Thrust and drag changes with airspeed

The estimated maximum speed V_{max} can be obtained by introducing the thrust and resistance formulas, thus obtaining

$$Distance_{max} = V_{max} * 90$$

3.5.5 Analyze Results

We conducted an exhaustive search of design parameters, including wingspan, weight, and wing area, considering all possible design options within our premise. We excluded extreme solutions where the climb rate during takeoff would be too low to reliably complete the competition. Using these solutions, we determined the highest score for each individual project, then we subsist them into the scoring formula.

$$Score = 1000 \times (\frac{P_{team}}{P_{max}} + \frac{E_{team}}{E_{max}} + \frac{D_{team}}{D_{max}})$$

Result is as follows
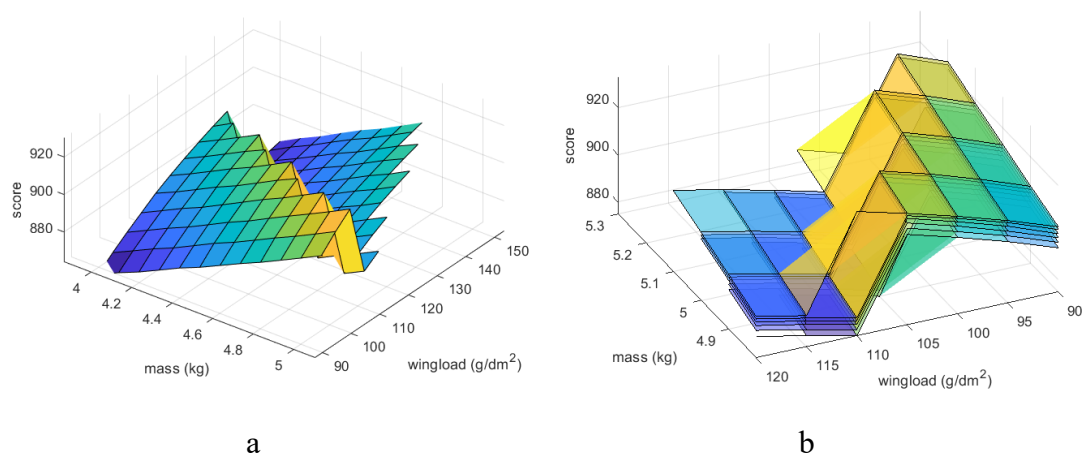
a
Cloud diagram of performance, takeoff mass and wing load distribution

b
Cloud diagram of scores for different wingspans (2.0-2.5m)

Figure 3.5.5

14

It can be seen that increasing the load capacity and reducing the wing area have significant advantages in scoring. From Figure 3.5.5, it can be seen that the 5% bonus is crucial for the selection of design points. Taking this bonus into consideration, we chose the point with the highest score within the safety range, which corresponds to a takeoff weight of 5kg and a design wing loading of 100g/dm². At the same time, from Figure 3.5.5-b, it can be seen that within the restricted range, the scores are not significantly affected by changes in wingspan. Therefore, for ease of design, a wingspan of about 2.1-2.3m is all acceptable.

At the same time, we have determined that our takeoff distance is 34m, our climb rate within 30s of takeoff to reach a height of 72m, and our optimal cruise speed for the efficiency flight phase is approximately 26m/s and the estimated score is 924.

4 Aerodynamic Design

4.1 Airfoil Design

Based on the results of the parameter sweep, we have learned that the aircraft operates at high speeds for the majority of the competition. Therefore, designing a clean wing profile for such conditions is advisable, and adopting a high-cambered wing profile with upwardly tilted flaps, for example, would be unwise. Additionally, due to the higher flight speeds, we may not necessarily need excessively cambered wing profiles. Using overly thin airfoils to reduce drag coefficient may also compromise our stall resistance. Moreover, based on past experience, the reduction in drag from such thin airfoils is only marginal.

From this, the previous constraints can be brought to a qualitative conclusion, that is, within a certain range, the increase in flight speed directly leads to the improvement of the overall performance, so a low-drag airfoil with a small camber should be designed. Select an airfoil with appropriate relative thickness and camber in the airfoil library and place it in Xoptfoil for optimization at $CL = 0.2$, so that the entire airfoil does not stall when the flaps are lowered to 10°, and the competition airfoil is obtained. The new airfoil and naca0009 polar curve are as follows $(Re = 5 \times 10^5)$
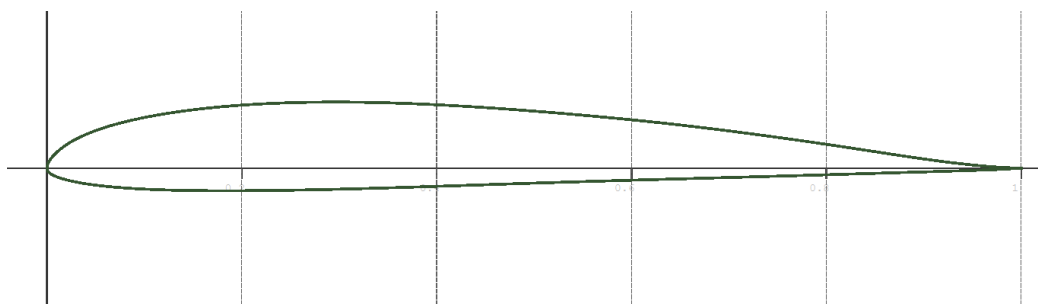

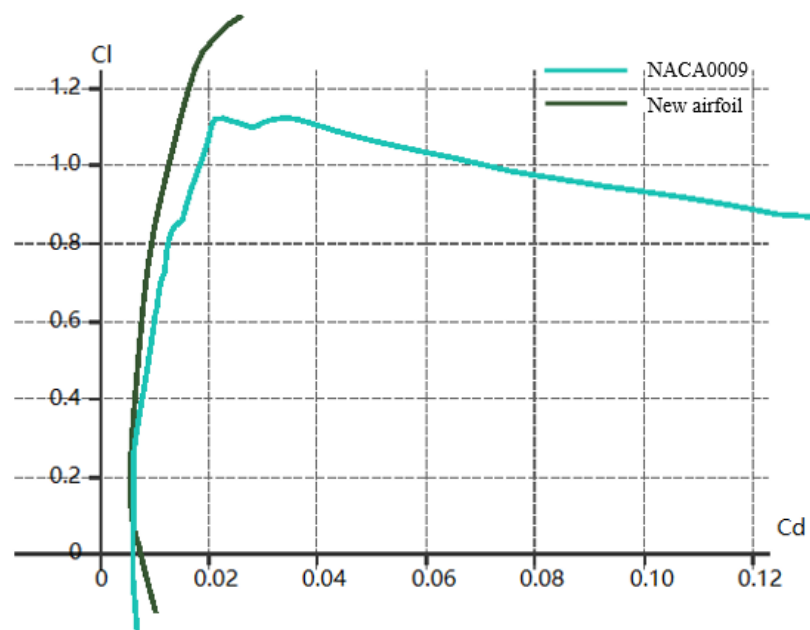Figure 4.1-1 New airfoil optimized by Xoptfoil

Figure 4.1-2 Comparison between the optimized airfoil and NACA0009

It can be found that the drag coefficient near the design lift coefficient is similar to the original estimate, so the previous estimation method is reliable.

4.2 Wingspan and Wing Area

At the same payload, a larger wingspan also results in better climb rate and lower turn-induced drag. Additionally, a larger wingspan results in a larger payload and thus a higher score. The range of wing span choices is given as 2.1-2.3m in Section 3.5.5. Here, for processing reasons (most carbon tubes and wood lengths available to us do not exceed 1m), we choose a single-wing length of 1050mm (900mm wing + 150mm wingtip).

At the same time, according to the optimization results, the load capacity of 5kg and the wing load of $100g/dm^2$ are selected as the design points. At this time, the wing area is about $0.500m^2$ and the chord is 250mm.

4.3 Wing Geometry

For a general model aircraft, the differences between an elliptical wing, a trapezoidal wing, and a rectangular wing with an added wingtip are minimal. Designing three aircraft with these different wing shapes, all with a control span of 2.1m and a wing area of 0.52m², the differences are subtle according to x5 calculations. Adopting other designs would result in wing chirality, doubling the workload for mold production. Therefore, for the sake of convenience in mold production, this aircraft's wing is designed as a rectangular wing with a swept wingtip. After x5 calculations, the maximum lift-to-drag ratio is still 26, which meets the requirements.
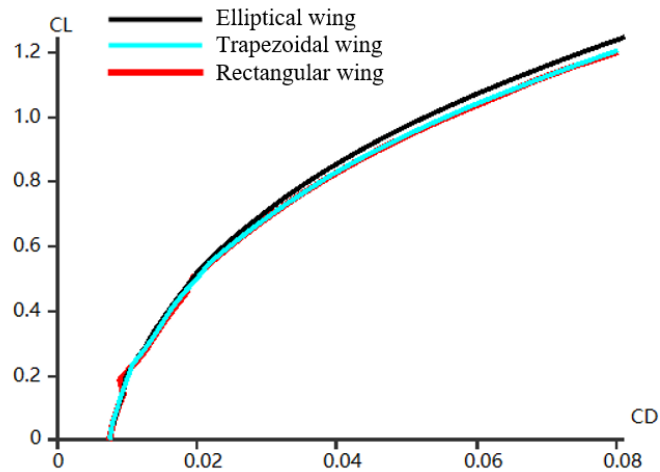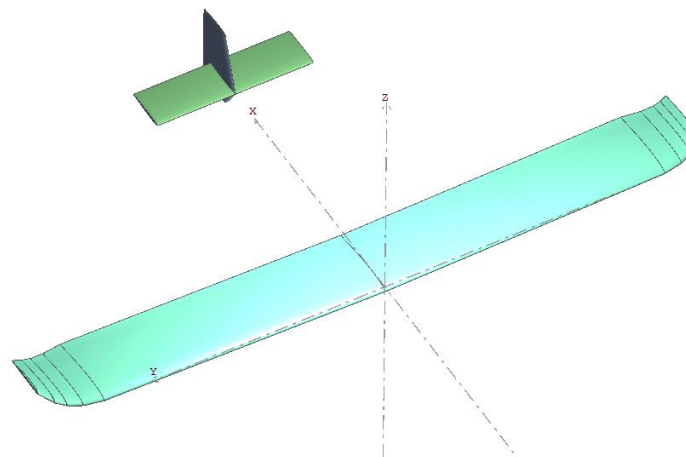
Figure4.3 Polar curves for different wing geometries
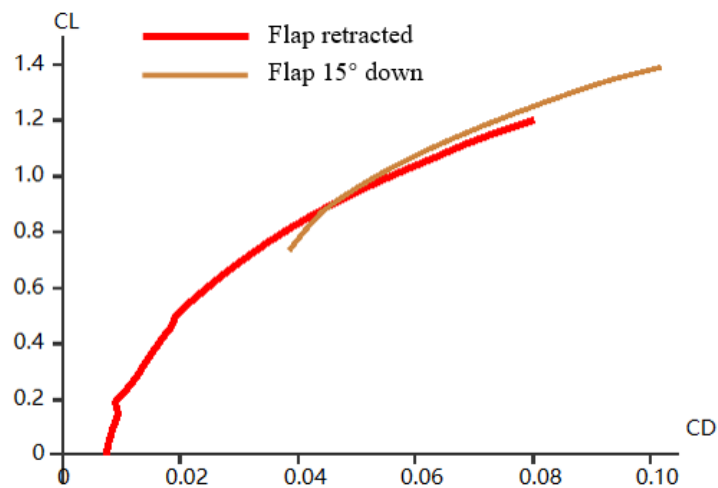

Figure4.3-1 aerodynamic shape of aircraft

Figure4.3-2 The polar curve of the aircraft

At the same time, from the calculation results, it can be seen that the maximum lift-to-drag ratio is achieved when $CL_{cruise} = 0.6$. Furthermore, when the flaps are deployed,

the CL of the aircraft can reach 1.2. This indicates that the parameters used for the global search are reasonable and achievable.

4.4 Fuselage

A streamlined fuselage is required for this competition. Considering aesthetics and drag reduction, we used a slightly modified NACA0009 airfoil to design our fuselage curve. We conducted CFD simulations to calculate the lift-to-drag ratio coefficients for three types of fuselage designs (as depicted in the figure below): the existing box-type fuselage, the semi-box-semi-tubular fuselage, and the tubular fuselage. The results are as follows (since viscous drag was already estimated, only pressure drag is considered here):
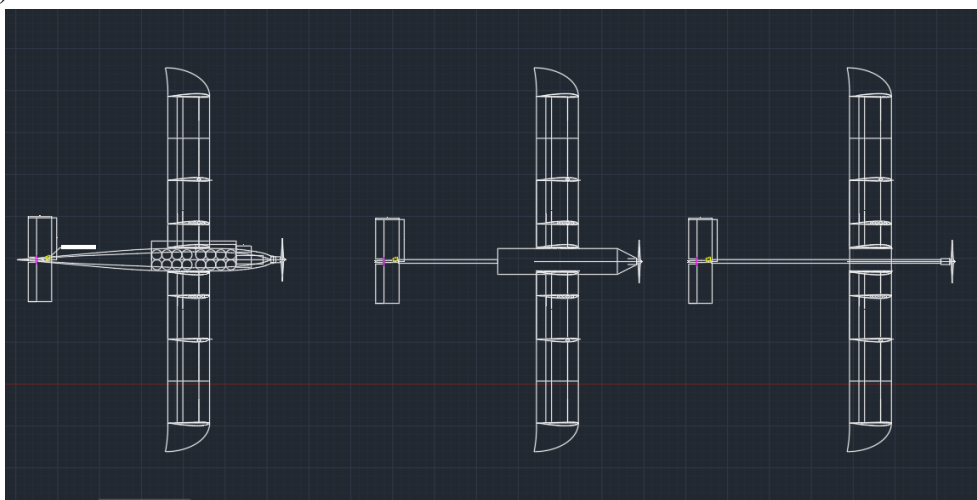

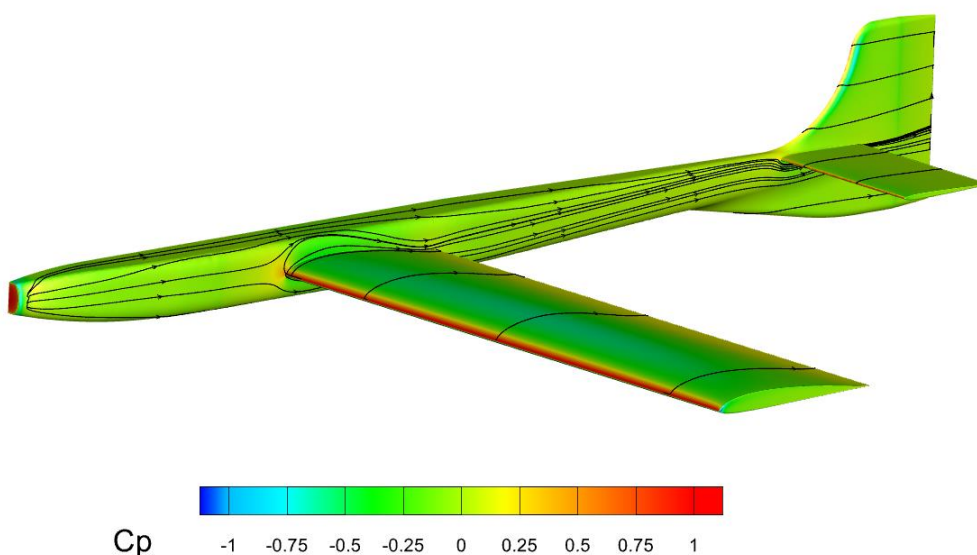
Figure4.4-1 Three types of fuselages used for analysis

Figure4.4-2 Figure 4.4-2: CFD Calculation Results for the Entire Aircraft

Fuselage/Force Coefficient	Streamlined Fuselage (currently used)	Tubular Fuselage	Semi-Box Semi-Tubular Fuselage
Lift Coefficient	0.613	0.576	0.587
Drag Coefficient	0.0397	0.0612	0.0387

Table4.4 Three types of fuselages CFD calculation results

These results verify that our fuselage design effectively enhances the overall lift-to-drag ratio while ensuring payload capacity through precise CFD analysis.

For more detailed information in structure, please refer to Section 6.2.

4.5 Landing Gear

Regarding the landing gear, initially, we aimed to use retractable landing gear to minimize drag. However, due to the thinness of the wing, with a maximum thickness of not exceeding 3cm, we found that commonly available worm gears on the market could hardly be fitted into the wing. Attempting to install them forcefully would create bulges on the wing, which we believe would result in more drag than a fully streamlined, lightweight landing gear. We also anticipate that it would introduce new unreliability issues. Therefore, we have decided to abandon this idea for safety reasons.

We have chosen a taildragger landing gear configuration for several reasons. Firstly, it has a smaller frontal area compared to a tricycle landing gear configuration, as it has one less exposed landing gear strut. Secondly, it avoids occupying space in the nose section of the aircraft. Thirdly, it complies with the requirement for a certain propeller ground clearance for grass field takeoffs and landings. Lastly, it allows for a larger angle of attack during takeoff, which helps in achieving a quick liftoff.
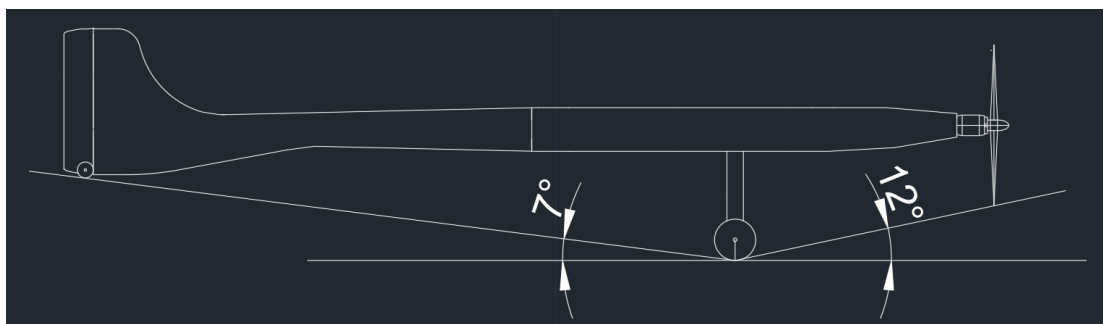

Figure 4.5 Landing Gear Geometric Dimension Design

5 Stability and Control

5.1 Stability and Static Margin

Due to the twisting of the wing, there are certain differences in longitudinal stability at different speeds, and the stability will decrease as the speed increases. The design center

of gravity is located near the center of pressure of the wing. Due to size restrictions, the length of the tail arm is about 0.9m. Considering the stability at each speed, the tail capacity is about 0.53, which can meet the stability requirements. CFD++ and xflr5 were used to analyze the main wing and tail wing, and the cruise longitudinal static stability margin was about 4.3%. The aircraft adopts a traditional layout, and there is generally no problem with stability in other directions.

5.2 Control

5.2.1 Pitch Control

Usually, the range of the elevator is 20%-30% of the tail area. This time we gave the tail arm a larger amount and used a full-motion horizontal tail to make the control more sensitive. We think this can achieve higher efficiency after takeoff.

5.2.2 Yaw Control

Similar to longitudinal control, a smaller rudder area can meet the requirements.

5.2.3 Roll Control

Assume that the wingspan is b and the flap length is b_0. Therefore, the roll moment generated by the aileron is:

$$\tau = \frac{b - b_0}{2} \frac{\rho v^2 S}{2} \delta Cl \frac{b}{b_0}$$

δCl: The difference between the maximum positive deflection and the maximum negative deflection lift coefficient of the aileron.
The aerodynamic damping in the roll direction is defined as the reverse roll moment generated by the roll angle ω. We assume that the lift line slope of each section is 2π/rad.

$$\gamma = \frac{2}{\omega} \int_0^{\frac{b}{2}} x * \frac{\rho v^2 S}{2} * 2\pi \frac{\omega x}{v} * \frac{dx}{b} = \frac{\pi}{12} \rho v^2 S b^2$$

For composite wings, the weight of the wing is approximately proportional to the area, with a proportional coefficient α. Therefore, the moment of inertia in the rolling direction is:

$$I = \frac{m_{wing} b^2}{12} = \alpha \frac{S b^2}{12}$$

Therefore, the equation of motion can be simplified to:

$$\ddot{\theta} = \frac{3\rho v^2 \delta Cl}{\sigma} \frac{(b - b_0) b_0}{b^3} - \frac{\pi \rho v}{\sigma} \cdot \dot{\theta}$$

Using initial value conditions, the ordinary differential equation can be solved as follows:

$$\theta = \frac{3\rho v \delta Cl}{\sigma} \frac{(b - b_0)b_0}{b^3}\left(t - \frac{\sigma}{\pi\rho v}e^{-\frac{\pi\rho v}{\sigma}t}\right)$$

The time constant $t = \sigma/\pi\rho v = 0.01317$ is very small, so the exponential term can be ignored when $\theta = \pi/3$.

Define $b = 2.2, v = 25m/s, \delta Cl = 1.2, \sigma = 1.2kg/m2, \rho = 1.16kg/m^3$ to calculate and to observe the relationship between b_0 and time.
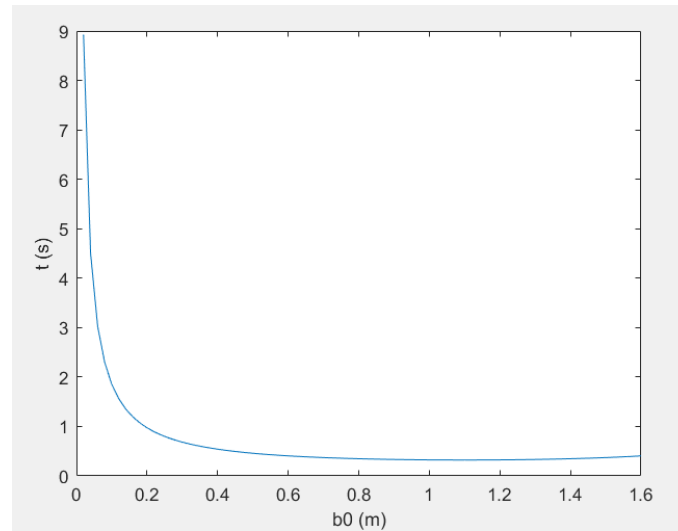

Figure 5.2.3 Relationship between flap length b_0 and response time t

In order to ensure sufficient rolling moment, we set the 1000mm (0.44 times span) length of the wing as flaperons and the inner part as flaps.

6 Structural Design and Manufacturing Techniques

6.1 Main Wing

The main wing that needs to be produced has a span length of 2.1m (excluding the fuselage width of about 0.13m), and is composed of 900mm rectangular sections at both ends and two small wings. For the rectangular wing section, we chose a monocoque wing made of foam sandwich composite material, and we processed a set of wood-substitute resin molds ourselves. At the same time, we directly use the method of pasting Teflon film for demolding, which can avoid relatively heavy mold grinding and polishing, and it is extremely easy to demold. For the main beam of the wing, we directly designed it as a complete carbon tube, which allowed us to avoid designing a pin with a risk of damage and greatly simplified our production process.

The wing shells adopts the currently most commonly used sandwich structure (Figure 6.1-1), with the skin consisting of 10g/m² carbon fiber chopped strand mat on the outside, 30g/m² 1mm PMI foam core in the middle, and 19g/m² glass fiber on the inside.

The use of carbon fiber chopped strand mat on the surface allows for a perfect fit to the curved surface, creating a rich resin layer on the wing surface, which is beneficial for later processing and polishing, and eliminates the need for painting. The 1mm PMI foam core provides sufficient thickness to the skin. The innermost layer of glass fiber fabric, together with other layers, forms a sandwich structure, providing rigidity and strength.
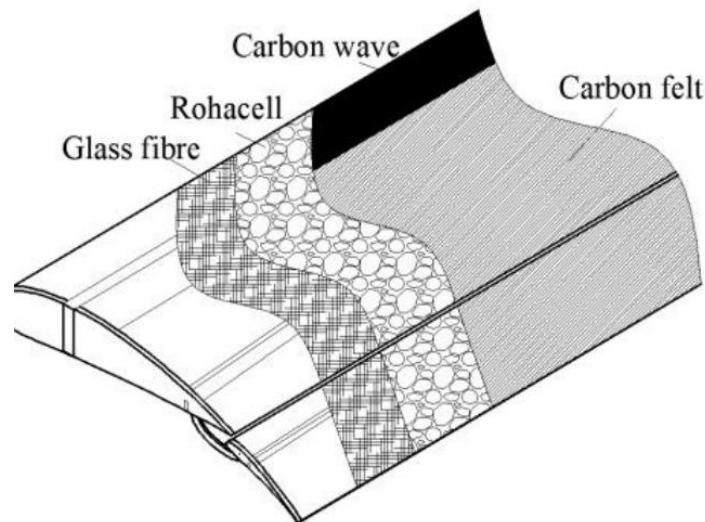

Figure6.1-1 lay-up of the wing shells

a
Processed wood substitute mold covered with Teflon cloth

b
The completed main wing.

Figure 6.1

For the winglets, we temporarily use 3D printed ASA-Aero. The curved surface printed

with this material is very beautiful and the quality is acceptable, and it saves us the cost of opening another set of molds. If we have enough time later, we will try to make an elegant composite winglet.

Figure 6.1-2 Winglets produced by 3D printing

6.2 Fuselage

The role of the fuselage is to connect the wings, tail, landing gear and other components, carry electronic equipment used for flight, and carry our 57mm diameter billiard passengers, so it needs sufficient bending strength and sufficient loading space. We planned to load at least 14 balls, leaving room for 16 balls, which gave us room to adjust our center of gravity.

This competition requires a smooth fuselage. For aesthetic reasons, we used a simply modified NACA0009 to draw our fuselage curves. At the same time, the cover needs to be opened for loading and unloading billiard balls, and the data recording box is huge and flat. Therefore, we chose to make the upper and lower surfaces of the fuselage into a huge flat surface. This way our main landing gear is also very easy to install.

We arranged some thin carbon tube reinforcements near the upper opening cover to connect the central wing box and the carbon fiber reinforcement frame of the landing gear. At the same time, we made a mounting base of just the right size for the data recording box, which will connect with the battery and the landing gear. The ESC is placed together in the equipment compartment on the nose of the machine.

In order to meet the strength requirements, our fuselage is made of carbon cloth-glass fiber composite material, and it is given some color using the mold internal paint process. This is our first attempt to spray paint on the surface of the composite material so that it will not be damaged in the process. Streaking in the sky, it seems to be working pretty well so far.

Figure 6.2 The finished fuselage

We also did some strength tests on it, and the fuselage was still in good condition after adding a 7kg iron block.

6.3 Empennage

Since the side area of the fuselage is large, we also made a slightly larger vertical tail. This time we chose to make the vertical tail directly with the fuselage, using the same material as the fuselage. The rear landing gear is buried inside the vertical tail and its wheels and rudder are coaxially connected. This not only reduces the resistance of the tail wheel, but also reduces one moving part during the assembly process, which reduces the difficulty of production and assembly and avoids the installation process. When the vertical tail contacted the ground, the vertical tail was torn apart due to excessive friction.

The horizontal tail is made into a two-piece full-moving horizontal tail design in order to consider disassembly. It is driven by a tilted servo, which also reduces the difficulty of connection. At the same time, the full-moving tail horizontal tail means that the deflection angle of the rudder surface becomes smaller during pitching, and since the curvature of the flat tail airfoil remains unchanged, the drag caused will also be reduced, which will be more conducive to our flight.
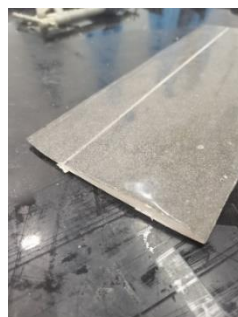

Figure 6.3 Vacuum bag composite sample

6.4 Landing Gear and Wheels

The landing gear is fixed under the front of the fuselage using carbon fiber brackets, and appropriate parking angles, anti-inversion angles and wheelbases are selected. The wheel is made of balsa wood covered with glass fiber and carbon fiber. It is milled and shaped, and the contact surface with the ground is coated with resin for reinforcement. The wheel shaft is made of carbon fiber tubes, and the connection between the bracket and the wheel shaft is fixed and reinforced with Kevlar fiber.

6.5 3D-Printing Mold

This year, due to considerations of economic cost and production time, we studied some experiences on the internet and developed our team's own process for 3D printing molds. Thanks to the maturity of consumer-grade 3D printers in recent years, we were able to print models with high surface quality without much adjustment. After appropriate painting and demolding treatment, the molds were ready to use.

We used this method to produce the fuselage, and it only took us 5 days to print and process the entire set of fuselage molds. The molds have good hardness (resistance to unnecessary deformation), light weight, and acceptable surface smoothness. Although they may not be suitable for long-term use, considering their total cost was even less than 50 euros and they allowed us to avoid CNC machining, we believe they are still very valuable.
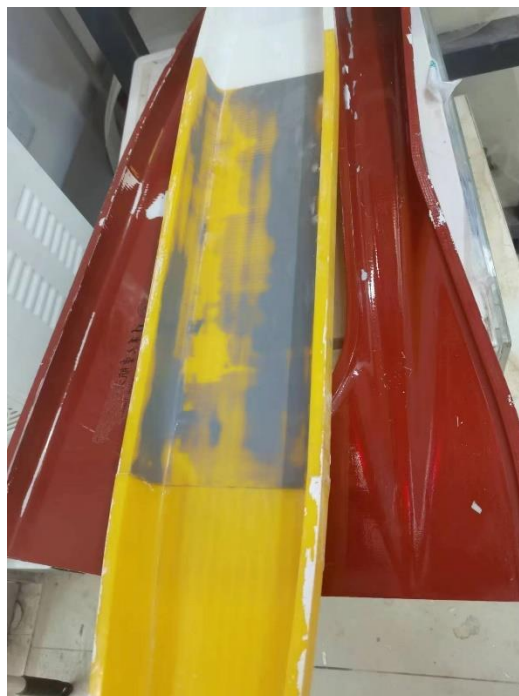
Figure6.5 the 3D-printing molds

6.6 Weight Estimate

Weight Estimation of Each part(g)

Component	Weight （g）
Motor + propeller	225
ESC + receiver, etc.	100
Battery	200
Measuring equipment	150
Fuselage + tail	500
landing gear	80
Wing	740
payload	2944 （184*16）
total	5000

Table6.6 Weight estimation

7 Payload Prediction

As demanded in the regulations the linear function for calculation of payload (kg) over air density ρ $(kg/m3)$ is given in the following equation. The required graph is given in Figure 7.1
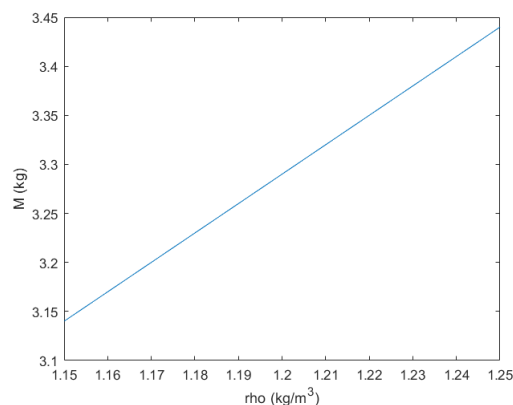
$$payload(\rho) = 1.69 + 3 * \rho$$

Figure7.1 Payload over air density

8 Current Progress

We conducted our first test flight at the end of March. The design at that time was still a rectangular wing in the middle section and a trapezoidal wing in the outer section.

The design point was the point in the lower left corner of Figure 3.6.4. At that time, our entire fuselage adopted 3D technology. Thanks to the process of combining printing and wooden skeleton, the weight is still controlled at about 2kg. During the test flight, we actually carried 11 balls, which is a load of about 2kg.

Figure 8-1 Verification aircraft

Figure 8-2 The attitude of the verification aircraft off the ground

According to measurements, the current in only a few intervals exceeds 30A during flight, and the maximum flight speed is about 27m/s, which basically meets the flight speed of about 30m/s we imagined at the time. Because the APC11*8 propeller is used, the flight speed is also It was observed that the takeoff was too smooth. Even when the pilot deliberately controlled the throttle and there was a tailwind, it only took about 20 meters to leave the ground, and the climb rate after leaving the ground seemed to have a margin, so we planned to the first test flight was replaced with an APC11*10 propeller in exchange for greater dynamic thrust.

9 Appendix

Registration form
3-view drawing
Isometric perspective view
Cargo bay

Registration form

Name	Gender	Date of Birth	Size of T-shirt	Remark
Ge/Dongyun	Female	1972.7.8	XL	Team Leader
Qian/Shiyu	Male	2002.7.16	L	Participant
Wang/Liuyi	Male	2004.6.5	XL	Participant
Su/Bohong	Male	2003.3.12	XXXL	Pilot
Chu/Zhijiang	Male	2004.3.6	XL	Participant
Li/Hongchen	Male	2002.11.29	XXL	Participant
Lei/Mingcheng	Male	2003.11.16	XL	Participant
Fu/Haochen	Male	2004.4.27	XXL	Participant
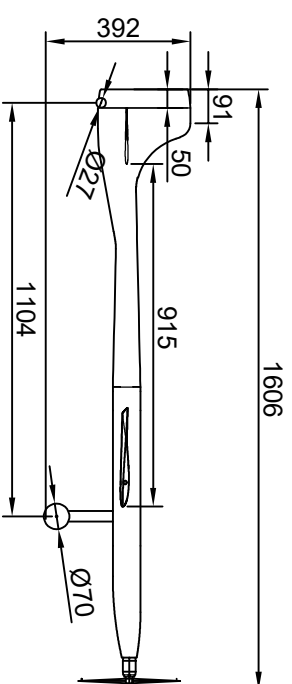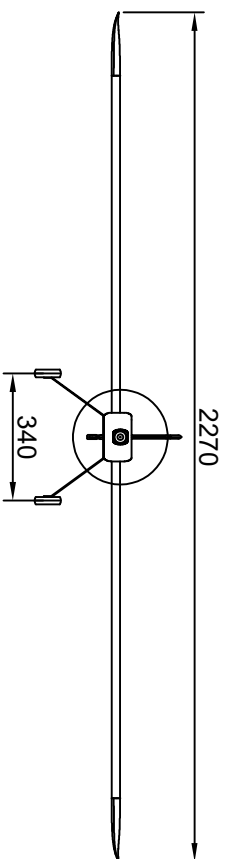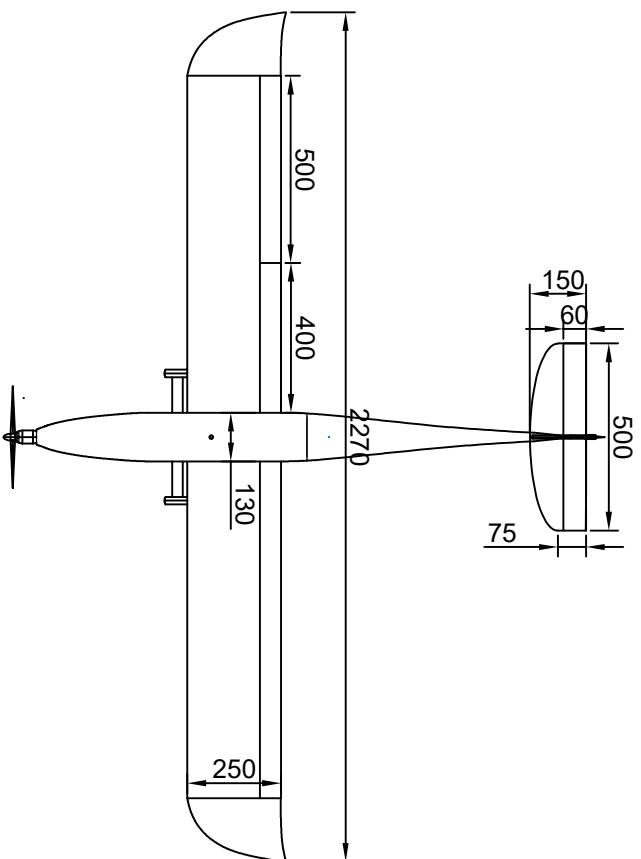
Detail Size Information of The Aircraft

Wing Span	2270mm
Wing Aera	0.515m^2
Length of Tail Moment Arm	2.27m
Fuselage Length	1606mm
Chord	250mm
Aspect Ration	9.08
Sweep Angle	0
Horizontal Tail Area	0.0666m^2
Vertical Tail Area	0.0538m^2
Tread	340mm
Wheelbase	1104mm
Volume of Cargo Bay	0.0044m^3

Air Cargo Challenge 2024	
Team Number: No.24	
Team Name: AIR	
Scale: 1/20	Page: 1/3

3-View Drawing

equipment cabin

measuring equipment

Cargo Bay

1020

90

190

24